PERGAMON

Current Opinion in Solid State and Materials Science 5 (2001) 45–53

Current Opinion in
Solid State &
Materials Science

A New Ti–15Zr–4Nb–4Ta alloy for medical applications

Yoshimitsu Okazaki*

Mechanical Engineering Laboratory, Agency of Industrial Science and Technology, Ministry of International Trade and Industry, 1–2 Namiki, Tsukuba, Ibaraki 305-8564, Japan

Abstract

V ions exhibit cytotoxicity in a culture medium from concentrations of ≧0.2 mg/L. Ti, Zr, Nb and Ta are biocompatible elements. A new Ti–15Zr–4Nb–4Ta alloy for medical implants is being developed. Its microstructure, mechanical properties, corrosion resistance and corrosion fatigue properties in a physiological saline solution, biocompatibility with cultured cells, new bone tissue response through rat tibia implantation and surface modification are discussed. Medical applications will be also addressed.

1. Introduction

Along with various implantable metals such as Co–Cr alloy and SUS316L stainless, the use of the Ti–6Al–4V alloy is increasing. Vanadium is classified in the toxic group and aluminium is classified in the capsule (scar tissue) group. Ti, Zr, Nb and Ta exhibit excellent biocompatibility and are in the loose connective vascularised (vital) group regards tissue reaction [1]. The giant-cell reaction appears around the polyethylene debris and wear particles of cement in failed total hip replacements when Ti–6Al–4V alloy is used. The giant-cell reaction increases with greater concentrations of the Ti, Al and V in the dry tissue [2]. The effects of various metal concentrations on cell viability using cultured cells have been examined using extracted mediums with various metal particles [3–5]. For V particle extraction, the relative growth ratios of L929 cells derived from murine fibroblastic tissue and murine osteoblastic MC3T3-E1 cells in Eagle's or α-medium extracts decreases when the V concentration in the medium increases to approximately 0.2–0.4 mg/L as summarized in Fig. 1. Moreover, as the quantity of released metallic ions into the medium are small (<0.3 mg/L) for Ti, Zr, Ta, and Nb particle extractions, the relative growth ratio of the L929 and MC3T3-E1 cells are equal to 1 (non-cytotoxicity). The effect of Al concentration on cell viability depends on surface roughness, surface treatment, strength of the Al oxide film and the extracting condition of the Al particles [4].

As an α+β type alloy not containing V, Ti–6Al–7Nb alloy is specified by the ISO 5832-11 standard. A near β type alloy, Ti–13Nb–13Zr alloy, is also specified in the ASTM F 1713-96 standard. Moreover, the β type Ti–12Mo–6Zr–2Fe alloy is specified in the ASTM F 1813-97 standard. This β type alloy has a slightly lower Young's modulus than the α+β type alloy. β type Ti–15Mo–5Zr–3Al and α+β type Ti–6Al–2Nb–1Ta alloys have been developed for advanced artificial hip joints by Kobe Steel Ltd. in Japan and are clinically used as artificial hip joints for cemented and cementless types, respectively [6–8]. In particular, for cementless artificial hip joints made of

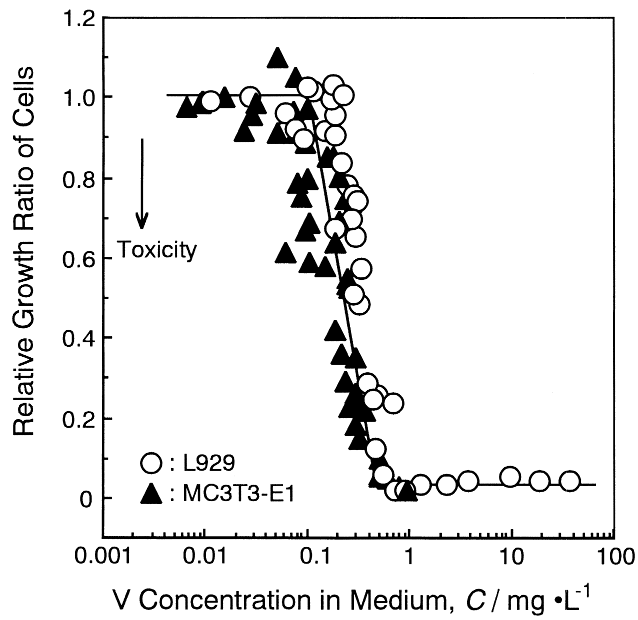

Fig. 1. Change in relative growth ratios of L929 and MC3T3-E1 cells as a function of V concentration in Eagle's and α-mediums.

*Tel.: +81-298-61-7179; fax: +81-298-61-7167.
E-mail address: m4610@mel.go.jp (Y. Okazaki).

1359-0286/01/$ – see front matter
PII: S1359-0286(00)00025-5

Table 1
Comparison of mechanical properties for new Ti–15Zr–4Nb–4Ta alloy annealed and aged after solution treatment at room temperature

	0.2% Proof strength $\sigma_{0.2\%PS}$/Mpa	Tensile strength σ_{UTS}/Mpa	Total elongation (%)	Reduction of area (%)	Young's modulus E/Gpa
Annealing	877	881	27	59	100
S.T.+Aging	918	1026	14	51	97

Ti–6Al–2Nb–1Ta, a part of the neck in the stem surface is improved by titanium plasma spray coating in combination with a bottom coating of apatite–wollastonite-containing glass–ceramic, which enables stable bone contact sooner after implantation. Ti–15Zr– 4Nb–4Ta alloy with biocompatible elements other than V and Al has been developed for medical implants in Japan. In this review paper, its mechanical and biological properties needed for medical applications will be summarized.

2. Microstructure and mechanical properties

The new Ti–15Zr–4Nb–4Ta alloy containing 0.2%Pd, 0.2%O, 0.05%N (hereafter called Ti–15–4–4 alloy) is melted by vacuum-arc melting. Beta transus and density of its alloy are 795°C and 4.98 Mg/m^3 (g/cm^3), respectively. After β and α–β forging, the alloy is annealed for 2 h at 700°C. Also, the alloy is solution-treated at 755°C for 1 h and then water cooled. The solution-treated alloy is aged at 400°C for 8 h and then air cooled. Conventional annealed Ti alloy is mostly lath of α′ martensite, while the solution-treated Ti–15–4–4 alloy consists of the primary α phase and α′ martensite. The fine α phase precipitate is due to the aging after solution treatment. A good balance of strength and ductility is achieved when the fine α phase is uniformly distributed by the solution treatment and aging [9–13]. Comparisons of the mechanical properties at room temperature are summarized as Table 1.

3. Corrosion resistance

3.1. Immersion test

The rate of Ti ion release in the 5 mass%–HCl solution decreases with greater quantities of Pd, Zr, Nb and Ta. In particular, the Ti ion release decreases remarkably with the addition of 0.2%Pd [9,11,12,14]. However, this Ti ion release is very small in the physiological saline solution.

3.2. Anodic polarization properties under static condition

When the current density measured by anodic polarization testing is low, the corrosion resistance of a metal is excellent. Anodic polarization curves of various metallic materials were compared in 5 mass%–HCl, 1 mass%–lactic acid (pH=2.5), phosphate buffered saline (PBS(−), pH=7.4), Eagle's medium (pH=8.4) and calf serum (pH=7.9) solutions at 37°C [11–16]. A passivation peak for Ti alloys is not observed except for 5 mass%–HCl, and the polarization curve immediately enters the passivity zone. The current density of the Ti–15–4–4 alloy in the high potential region (2 V vs. SCE) was the lowest compared to other metallic materials.

3.3. Corrosion resistance under wear condition

The anodic polarization curve under friction can be used to measure with a polarization cell as shown in Fig. 2 [17]. The specimen electrode is reciprocally moved by a cam which keeps it in contact with an apatite ceramic. The applied load is displayed digitally by the load cell and the frictional load is adjusted with screws. To maintain the testing solution at 37°C, hot water is circulated around the cell. The reciprocal speed is varied by changing gears and the ratio of teeth in the gear box. The cell is made of Teflon, and the holder for the ceramic is made of polychloro tetrafluro ethylene (PCTFE, Daiflon). Test specimens 10 mm in diameter and 10 mm in thickness were prepared from the sample alloy. After connecting a test specimen to a platinum wire by means of a lug terminal and screw, it is inserted into daiflon, and, except for 0.8 cm^2, the specimen surface is covered with epoxy resin. Thereafter, the specimen surface was polished with waterproof emery paper up to 600 grit under running water, followed by cleaning in an ultrasonic bath of ethanol. The reciprocal distance was 5 mm, apatite ceramic was used for the friction specimen to simulate bone tissue, the data collecting interval was 2 s, the reciprocal speed at 10^{-2} m/s (1 Hz), and the frictional load was up to 59 N. After the specimen electrode and the friction specimen were set in the polarization cell, the testing solution was deaerated with high-purity nitrogen at a rate of 1.67×10^{-6} m^3/s for 0.6 ks. The specimen was initially held at −1.5 V for 300 s. An anodic polarization test was then carried out from −1.5 V to 5 V at a sweep rate of 40 mV/min with a small amount of high-purity nitrogen gas flowing over the solution surface. During the anodic polarization test, the measurements were taken by adjusting the screws to minimize frictional load fluctuation. Fig. 3 shows comparisons of anodic polarization curves under a static condition and the mean frictional load of 49 N at a frequency of 1 Hz with the apatite ceramic in the Eagle's medium solution at 37°C. The current density under

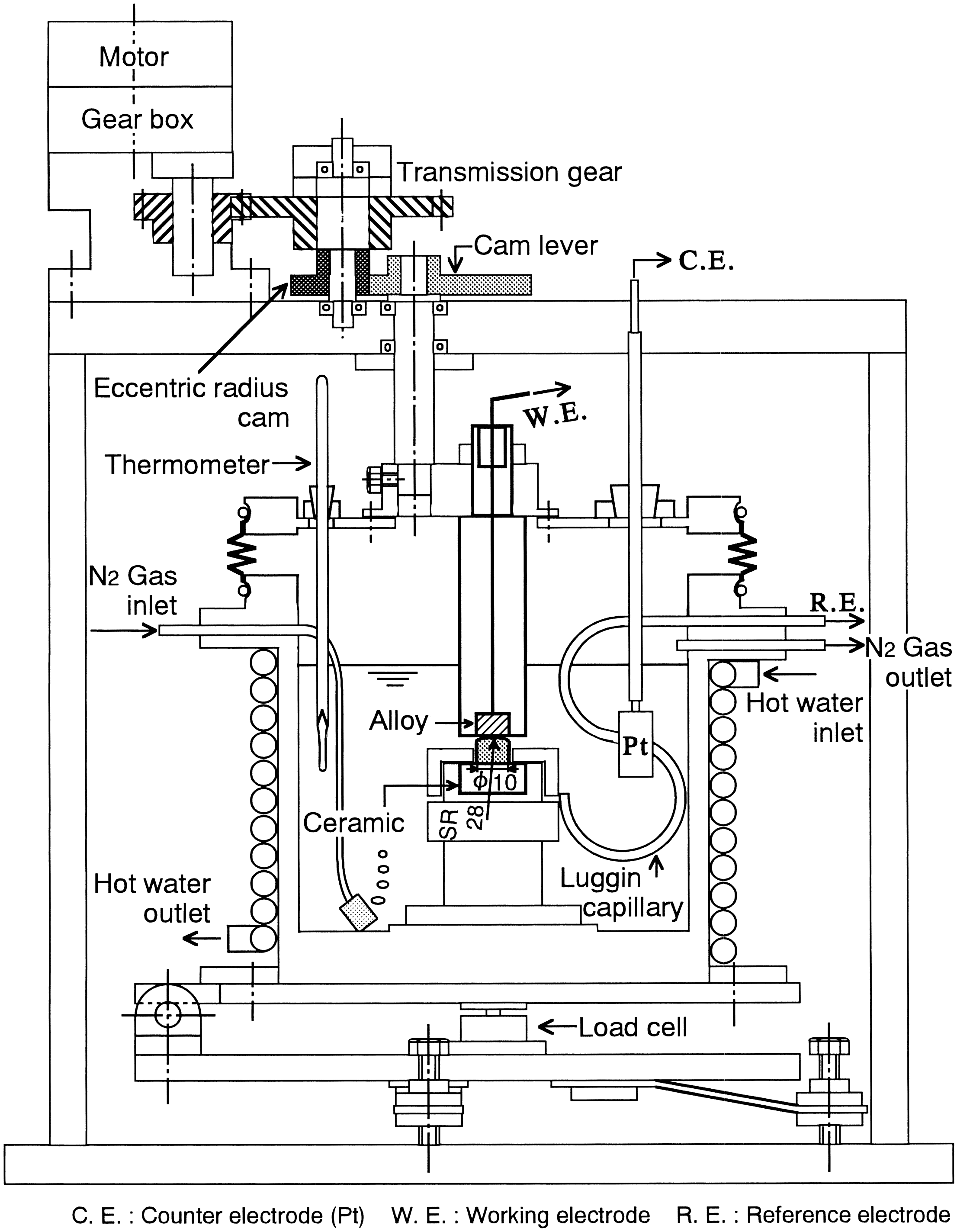

Fig. 2. Schematic diagram of polarization cell for anodic polarization test under friction.

friction was higher than that of the static state and fluctuated with the destruction and formation of the passive film. For SUS316L stainless steel and Co–Cr alloy, fluctuation of the current density is seen only in the passivity zone, but almost no fluctuation is seen in the active and transpassive zones. With Ti alloys, fluctuations of the current density arising from friction are seen from the activity zone to the high potential region, increasing in fluctuation widths of current density and the mean current density. Especially, in the case of the new Ti–15–4–4 alloy, as shown in Fig. 3(d), the fluctuation of the current density remained small up to the high-potential zone. The SUS316L stainless steel and the Co–Cr alloy showed a small decrease in corrosion potential (open circuit potential) in spite of the increased frictional load. While, the Ti alloys tend to decrease.

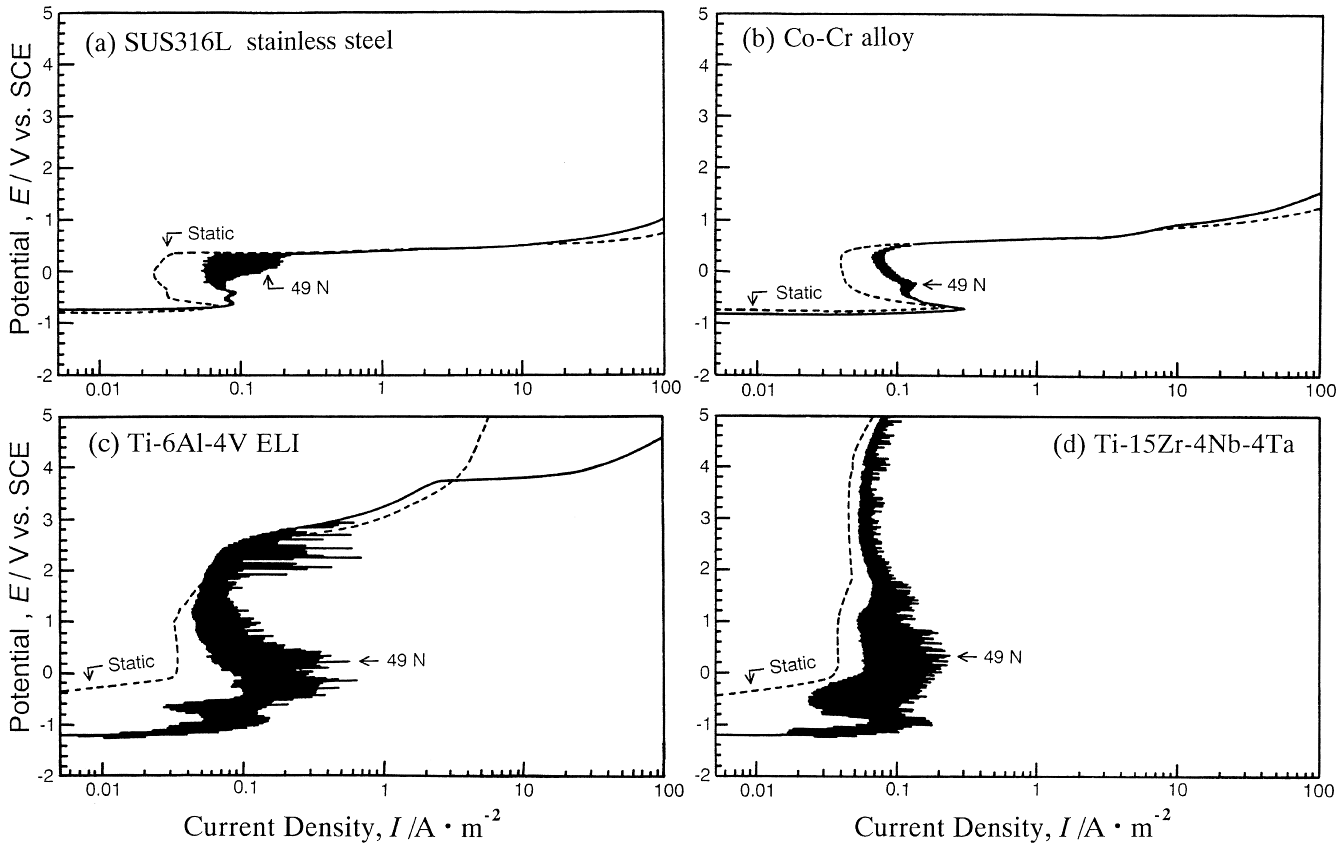

Fig. 3. Effect of 49 N kinetic frictional force on the anodic polarization curves with apatite ceramic for various implant alloys in Eagle's medium solution at 37°C. (a) SUS316L stainless steel, (b) Co–Cr alloy, (c) Ti–6Al–4V ELI, (d) Ti–15Zr–4Nb–4Ta alloy.

3.4. Role of alloying elements in passive films

The effects of the alloying elements in passive films were examined by X-ray photoelectron spectroscopy (XPS) [14,17]. The passive film surface formed on Ti–15–4–4 alloy consists mainly of TiO_2, with trace quantities of Ti_2O_3, ZrO_2, Nb_2O_5 and Ta_2O_5. The Pd is close to the peak of PdO.

4. Corrosion fatigue properties

The corrosion fatigue test was carried out in Eagle's medium solution [13,18]. To make the oxygen concentration in the medium solution closer to the condition in a living body and to maintain the pH at 7.4, a small amount of $90\%N_2+5\%CO_2+5\%O_2$ mixed gas was bubbled into the medium solution. The fatigue test conditions were: a sine wave with a stress ratio (R=(minimum tensile stress)/(maximum tensile stress)) of 0.1, a frequency of 10 and 2 Hz, and a number of cycles up to 10^9 times. Fatigue tests using a load profile estimated from the analysis of forces and movements of a human hip joint (called a hip joint load profile) shown in Fig. 4(d) were also conducted. Fig. 5 shows a comparison of S–N curves obtained from the corrosion fatigue tests with the sine wave and a hip joint load profile. The number of cycles-to-failure for the annealed Ti–15–4–4 alloy increased as the maximum stress decreased, and it was found that rupture stress at 10^8 cycles coincided at approximately 600 MPa. The effects of frequency on the fatigue strength at 2 and 10 Hz were almost similar, and the fatigue strengths were the same for the sine wave and human hip joint load profile.

5. Biocompatibility

5.1. Cytocompatibility for Ti alloy plate

Two types of cells were used: L929 cells derived from murine fibroblastic tissue and murine osteoblastic MC3T3-E1 cells. A Ti–6Al–4V ELI (extra low interstitial) alloy plate was used as the control. The relative growth ratios of the L929 and MC3T3-E1 cells were estimated using the following formula: (average number of cells per dish after 4 d incubation)/(average number of cells in the control). The relative growth ratios of the L929 (1.09 ± 0.04) and MC3T3-E1 (1.08 ± 0.02) cells for the Ti–15–4–4 alloy were slightly higher than those of the Ti–6Al–4V ELI alloy [18,19].

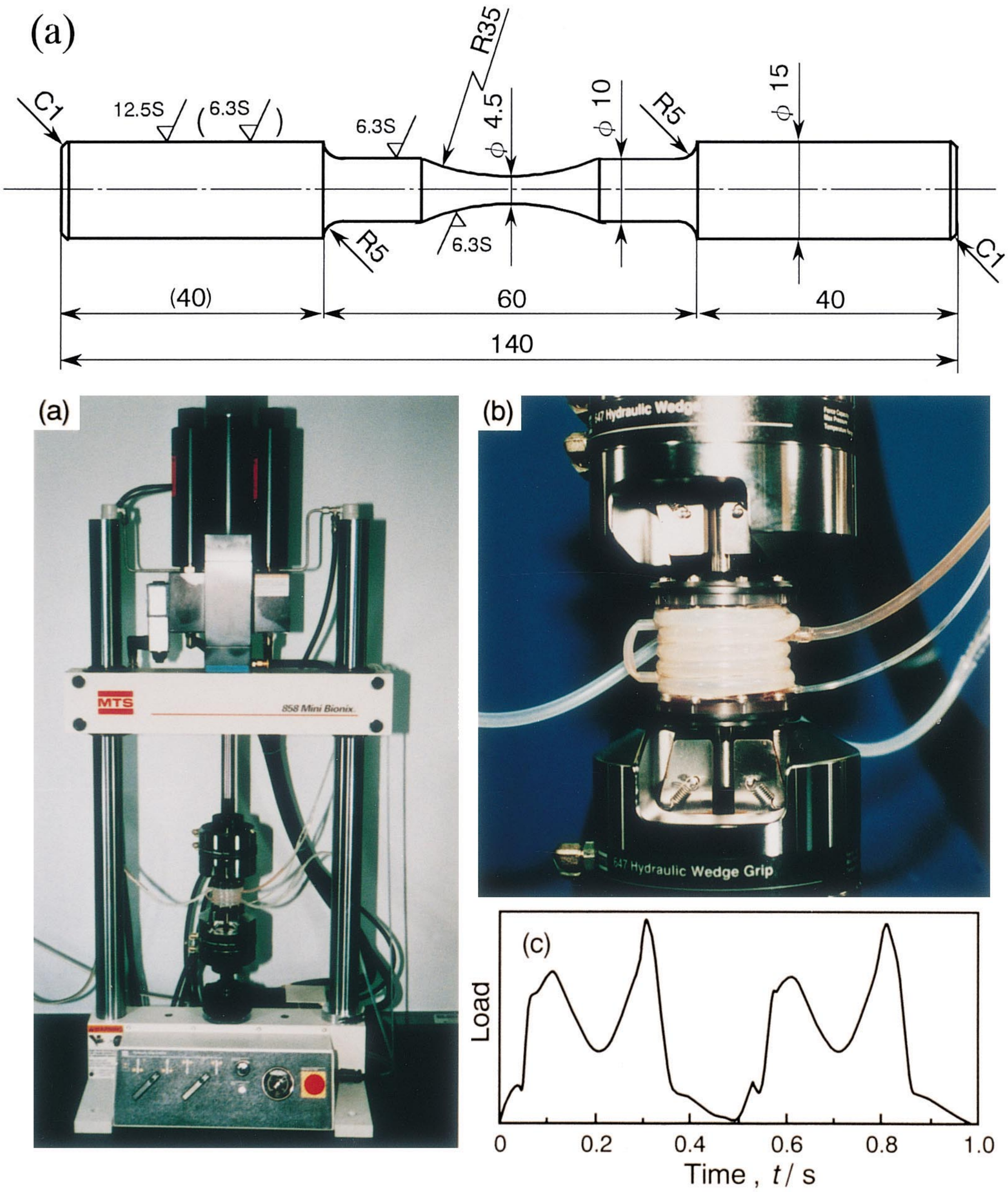

Fig. 4. Dimensions of test specimens (a) and MTS model 858 Mini Bionix equipment (b), cell (c) and hip joint load profile (d) used in corrosion fatigue tests.

5.2. Cytocompatibility with Ti alloy wear powder

The Ti alloy disk was worn with pin of apatite ceramic in Eagle's medium [20]. Wear powder sterilized in ethanol was added to the culture medium. The relative growth ratios of L929 and MC3T3-E1cells for the Ti–6Al–4V alloy wear powder decreased below that of the Ti–15–4–4 alloy wear powder. The concentration of V released from the wear powder into the medium increased moderately with increases of wear powder. This effect was approximately in agreement with the results estimated from medium extraction with high-purity V particles. For the Ti–15–4–4 wear powders, the maximum Ti concentration released from the wear powder was approximately in agreement with the results obtained with high-purity Ti particles. On the contrary, for Zr, Nb and Ta the maximum metal concentrations released from the wear powders were much lower than those obtained with high-purity metal particles.

5.3. New bone tissue formation using rat tibia implantation

Ti–15–4–4 and Ti–6Al–4V ELI alloy implants (1.2 mm in diameter and 2.0 mm in height) were implanted into

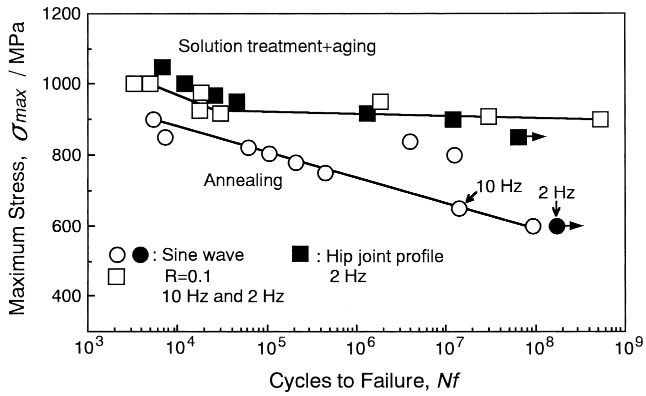

Fig. 5. Comparison of S–N curves obtained by corrosion fatigue tests with sine wave and hip joint load profiles for new Ti–15Zr–4Nb–4Ta alloys annealed and aged after solution treatment in Eagle's medium solution at 37°C.

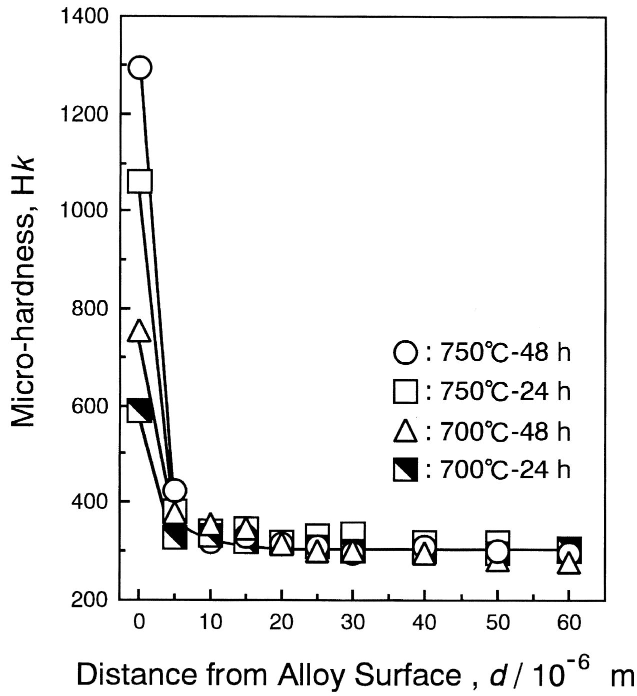

Fig. 7. Change in micro-hardness toward inside from new Ti–15Zr–4Nb–4Ta alloy surface nitrided with high-purity nitrogen gas at 700°C and 750°C for up to 48 h.

the bone marrow of the left and right sides of the tibiae for 6, 12, 24 and 48 weeks. Non-decalcified optical micrographs for the Ti–15–4–4 and Ti–6Al–4V alloys 12 weeks after implantation are shown in Fig. 6. New bone formed well around the Ti alloys implanted in the bone marrow. The newly formed bone around the new Ti–15–4–4 alloy tended to be slightly thicker than that around the Ti–6Al–4V alloy. For the Ti–6Al–4V alloy, pits perpendicular to the polishing direction caused by corrosion tended to increase with longer implantation times.

6. Surface modification by nitriding

The specimen surfaces (15 mm in diameter and 10 mm in thickness) were polished with waterproof emery paper up to 1000 grit under running water, followed by cleaning in an ultrasonic bath of ethanol and acetone. The Ti alloy specimens were nitrided at 700 and 750°C for up to 48 h using high-purity (99.999) nitrogen gas of 0.1 MPa (1 atm) [22]. The micro-hardness (load: 25 g) was measured toward the inside from the alloy surface. Fig. 7 shows the changes in the micro-hardness. Except for the Ti alloy surface, micro-hardness in this figure is micro-Knoop

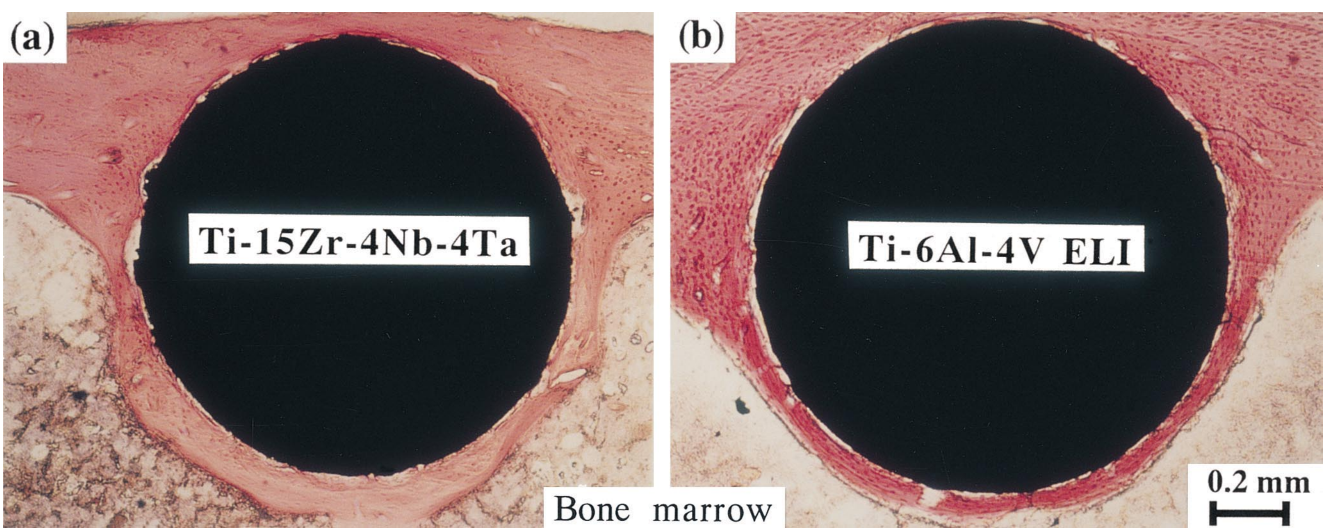

Fig. 6. Optical micrographs of non-decalcified sections of new Ti–15Zr–4Nb–4Ta alloy (a) and Ti–6Al–4V ELI (b) alloys stained with Azan–Mallory stain 12 weeks after implantation.

hardness. The micro-Vickers hardness at the alloy surface is high, and it increased with longer nitriding time. The thickness of the nitrided layer after 48 h at 750°C was less than 5 μm.

7. Medical applications

7.1. Surgical and orthopedic application

Bone plate, artificial hip joints of the cementless type and artificial teeth roots can be trial-manufactured with the Ti–15–4–4 alloy as shown in Fig. 8. The surface of the bone plate is modified by anodic oxidation. A part of the neck in the stem surface of the artificial hip joints shown in Fig. 8 (b) is modified by the same method as advanced artificial hip joints (cementless type) made of Ti–6Al–2Nb–1Ta alloys.

7.2. Dental prosthetic application

The mechanical properties of dental castings centrifugally cast with Ti–15–4–4 alloy were evaluated by tensile testing at room temperature [23]. The 0.2% proof strength and ultimate tensile strength were 739±53 MPa and 915±51 MPa, respectively. The total elongation and reduction of area were 7±2% and 8±6%, respectively. Anodic polarization properties in 1% lactic acid and artificial saliva (pH=5.7) solutions were same as that of annealed alloy. A metal plate for complete denture, partial dentures, crown and bridge using the Ti–15–4–4 alloy can be made as shown in Fig. 9.

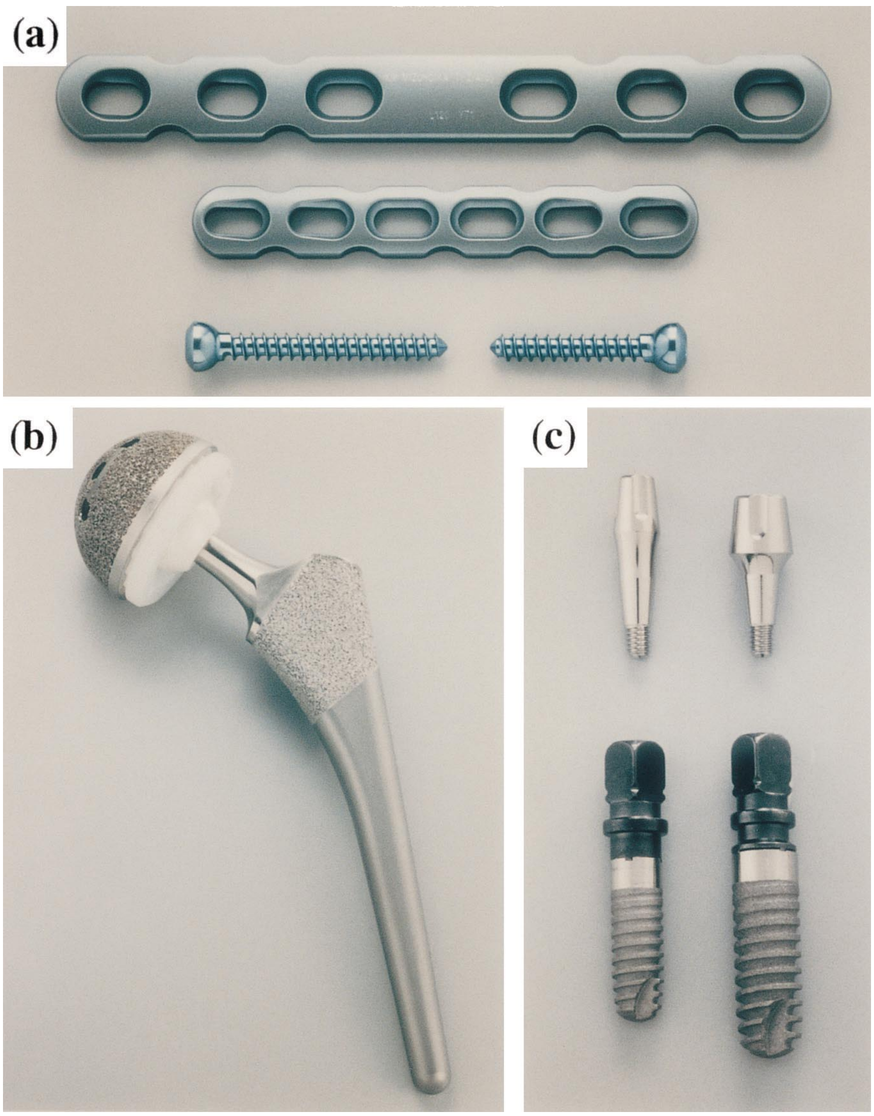

Fig. 8. Bone plate (a), artificial hip joint of cementless type (b) and artificial teeth root (c)made of new Ti–15Zr–4Nb–4Ta alloy.

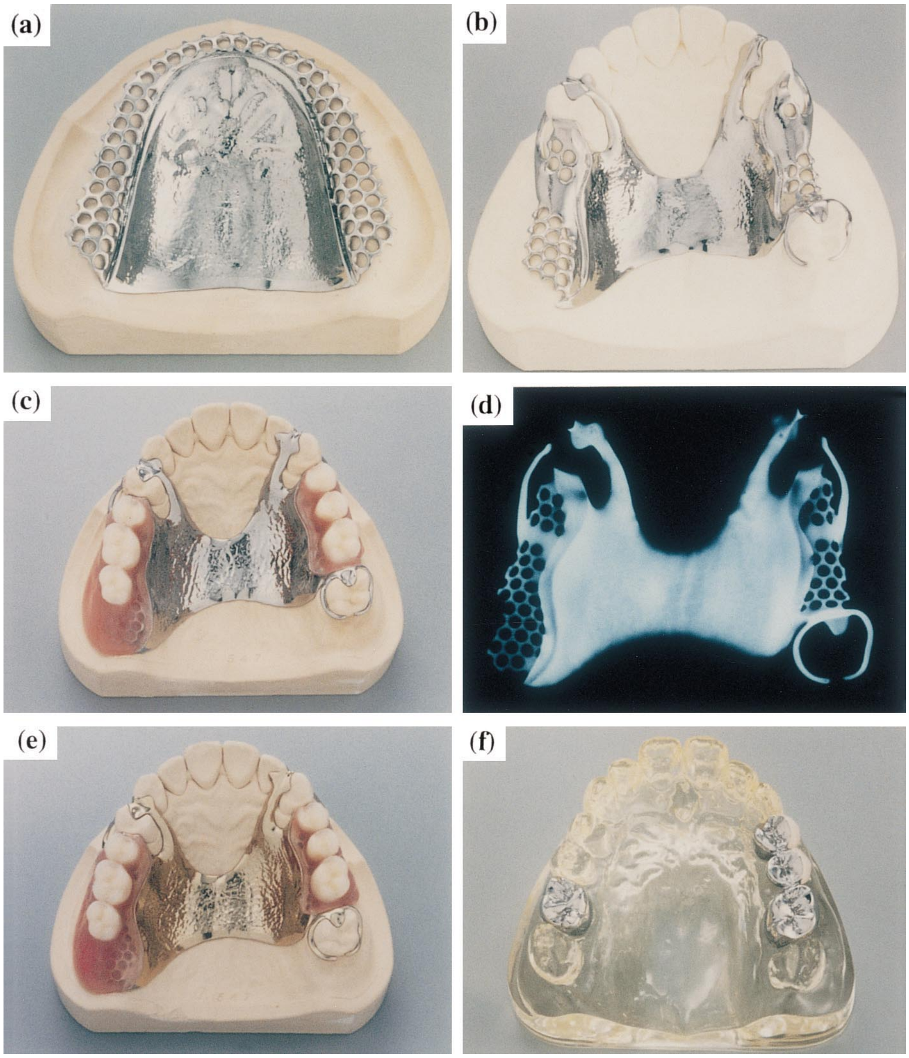

Fig. 9. Metal plate for complete denture, partial denture, crown and bridge made of new Ti–15Zr–4Nb–4Ta alloy. (a) Metal plate for complete denture, (b) metal plate for partial denture, (c) partial denture, (d) radiograph of metal plate for partial denture, (e) TiN ion-plated partial denture, (f) crown and bridge.

8. Conclusion

The new Ti–15Zr–4Nb–4Ta alloy with its excellent mechanical properties, corrosion resistance and corrosion fatigue properties and biocompatibility can be expected to become a new alloy for medical applications in the future.

References

[1] Steinemann SG. In: Winter GD, Leray JL, de Goot K, editors, Evaluation of biomaterials, Chichester: Wiley, 1980, pp. 1–34.
[2] Agins HJ, Alock NW, Bansal M, Salvati EA, Wilson Jr PD, Pellicci PM, Bullough PG. Metallic wear in failed titanium alloy total hip replacement. J Bone Joint Surg 1988;70–A:347–56.
[3] Okazaki Y, Rao S, Asao S, Tateishi T, Katsuda S, Furuki Y. Effects of Ti, Al and V concentrations on cell viability. Mater Trans JIM 1998;39:1053–62.
[4] Okazaki Y, Katsuda S, Furuki Y, Tateishi T. Effects of aluminum oxide film on fibroblast L929 and V79 cell viabilities. Mater Trans JIM 1998;39:1063–9.
[5] Okazaki Y, Rao S, Asao S, Tateishi T. Effects of metallic concentrations other than Ti, Al and V on cell viability. Mater Trans JIM 1998;39:1070–9.
[6] Matsuda Y, Nakamura T, Ido K, Oka M, Okumura H, Matsushita T. Femoral component made of Ti–15Mo–5Zr–3Al alloy in total hip arthroplasty. J Orthop Sci 1997;2:166–70.
[7] Ido K, Matsuda Y, Yamamuro T, Okumura H, Oka M, Takagi H. Cementless total hip replacement. Acta Orthop Scand 1993;64:607–12.
[8] Yamamuro T, Nakamura T, Iida H, Matsuda Y. A new model of bone-conserving cementless hip prosthesis made of high-tech materials: Kobelco H-5. In: Imura S, Wada M, Omori H, editors, Joint arthroplasty, Tokyo: Springer, 1999, pp. 213–24.
[9] Ito A, Okazaki Y, Tateishi T, Ito Y. In vitro biocompatibility, mechanical properties, and corrosion resistance of Ti–Zr–Nb–Ta–Pd and Ti–Sn–Nb–Ta–Pd alloys. J Bio Mater Res 1995;29:893–900.
[10] Okazaki Y, Ito Y, Ito A, Tateishi T. Effect of alloying elements on mechanical properties of titanium alloys for medical implants. Mater Trans JIM 1993;34:1217–22.

[11] Okazaki Y, Ito Y, Ito A, Tateishi T. New titanium alloys to be considered for medical implants. In: Brown SA, Lemons JE, editors, Medical applications of titanium and its alloys: the material and biological issues, astm stp 1272, ASTM, 1996, pp. 45–59.
[12] Okazaki Y, Ito Y, Tateishi T. Effects of heat treatment on mechanical properties and corrosion fatigue strength in physiological saline solution of new titanium alloys for medical implants. Mater Trans JIM 1996;37:843–9.
[13] Okazaki Y, Ito Y, Kyo K, Tateishi T. Corrosion resistance and corrosion fatigue strength of new titanium alloys for medical implants without V and Al. Mater Sci Eng A 1996;213:138–47.
[14] Okazaki Y, Kyo K, Ito Y, Tateishi T. Effects of Mo and Pd on Corrosion resistance of V-Free titanium alloys for medical implants. Mater Trans JIM 1997;38:344–52.
[15] Okazaki Y, Ito A, Tateishi T, Ito Y. Effect of alloying elements on anodic polarization properties of titanium alloys in acid solutions. Mater Trans JIM 1994;35:58–66.
[16] Okazaki Y, Tateishi T, Ito Y. Corrosion resistance of implant alloys in pseudo physiological solution and role of alloying elements in passive films. Mater Trans JIM 1997;38:78–84.
[17] Okazaki Y, Kyo K, Ito Y, Tateishi T. Effect of friction on the corrosion resistance for implant alloys in physiological saline solution. J Japan Inst Metals 1997;61:1122–31. in Japanese.
[18] Okazaki Y, Ito Y. New Ti alloy without Al and V for medical implants. Adv Eng Mater 2000;2:278–81.
[19] Okazaki Y, Rao S, Tateishi T, Ito Y. Cytocompatibility of various metal and development of new titanium alloys for medical implants. Mater Sci Eng A 1998;243:250–6.
[20] Okazaki Y, Nishimura E. Effect of metal released from Ti alloy wear powder on cell viability. Mater Trans JIM 2000;41:344–52.
[22] Okazaki Y. Surface modification. In: Ichikawa K, editor, Functionally graded materials in the 21st century. A workshop on trends and forecasts, Kluwer Academic Publishers, 2000, pp. 191–5.
[23] Manabe T, Nakada H, Okazaki Y, Kobayashi K. Mechanical properties and corrosion resistance of dental cast Ti–15Zr–4Nb–4Ta alloy and trial fabrication of metal plates, crown and bridge. J Jpn Prosthodont Soc 2000;44:151–60. in Japanese.